Design of dual-band Wilkinson power divider based on novel stubs using PSO algorithm

Seyed Abed Zonouri, Mohsen Hayati [iD] and Mehran Bahrambeigi

Department of Electrical Engineering, Faculty of Engineering, Razi University, Kermanshah 67149, Iran

Abstract

In this paper, a new dual-band Wilkinson power divider (WPD) is designed and fabricated using novel low and high impedance stubs instead of quarter-wavelength transmission lines. The proposed circuit was analyzed using odd and even mode analysis, and the optimal values of design parameters were obtained using the particle swarm optimization algorithm. The designed power divider has input reflection coefficients (S_{11}) of −22.1 and −17 dB at the first operating frequency of 2.2 GHz and the second operating frequency of 14.2 GHz, respectively. It also improves stop-band and fractional bandwidth (FBW) while maintaining a simple topology. The proposed WPD suppresses undesired harmonics from the second to the fifth with an attenuation level of less than −20 dB in the first band and generates a broad stop-band (4.4–11.5 GHz). In the first band, the FBW is 54.5%, and in the second band, it is 20.1%.

Introduction

Microwave circuits are now a common component of wireless systems, and three-port power dividers (PDs) are a common component of microwave circuits. Conventional PDs can be used in microwave circuits, but their operational bandwidth is often limited. As a result, attaining an appropriate bandwidth is one of their design problems [1, 2].

The Wilkinson power divider (WPD) divides the input power evenly between the two output ports, ideally without losses, and can also function as a power coupler. The characteristics of a suitable WPD are the matching of ports, small dimensions, wide bandwidth, and isolated output ports [3].

A band-pass WPD is provided in [4], where the quarter-wavelength ($\lambda/4$) transmission lines are substituted by coupling lines. However, this method increases the circuit size compared to the conventional WPD. A WPD with open-circuit stubs at each port is used in [5] to eliminate harmonics with a high attenuation level. But, due to the high-frequency noise effect, the measured S parameters for the suppressed fifth harmonic have a fuzzy shift. Two triangular-shaped resonators, two open-circuit stubs, and a trapezoidal-shaped suppressor with a 68% attenuation and small dimensions are used in [6] to provide an ultra-wide PD. This WPD has a small size but is single-band and has limited applications.

Various techniques, such as rectangular-shaped resonators [7], circular-shaped resonators [8, 9], open stubs [10, 11], taper transmission lines [12], and coupled lines [13], have been used to design a PD by attenuating undesired signals and small dimensions. These structures are inefficient and complex, despite their excellent features.

On the other hand, the Gysel structure is one way to design a PD. Despite their excellent isolation and high thermal conductivity, Gysel structures have large circuit dimensions that limit their applications and suffer from complex architectures [14–16].

A two-way WPD with equal power division was proposed in [17] and featured a wide cutoff band and low insertion loss. Two impedance-matching lines and a two-sided composite transmission line is used in the design of this circuit. The proposed dual-band PD has two central frequencies at 0.90 and 2.45 GHz, making it suitable for RF/microwave applications. In [18], a dual-band WPD is developed based on an isolation network with additional lumped elements. This structure has six transmission zeros but is large and has an unsuitable in-band input reflection coefficient. Another compact dual-band coplanar WPD is presented in [19] which modified coplanar waveguides separated by a series stub. It is used to achieve two adjustable frequency bands. However, this circuit does not have a wide stop band. In [20], a compact structure is presented, which includes a short stub, three transmission lines, and lumped components (RLC). This PD operates at frequencies of 1 and 2.5 GHz, and due to the RLC circuit, it has high output matching and perfect isolation. But it does not reject spurious harmonics and has a fluctuated passband.

A series-in-phase 3-way dual-band PD is proposed in [21]. This divider is intended and implemented to operate at 0.915 and 2.440 GHz. Its design employs the composite right- and left-handed transmission lines technique. It has a low input reflection coefficient and an equal power split to the output ports in two bands. However, its bandwidth is limited. Additionally, there is no harmonic suppression.

In recent years, various methods have been used to improve the performance of PDs. In [22], the particle swarm optimization (PSO) algorithm and finite difference time domain methods are combined to achieve an optimal PD design for a suitable specification. But the PD is single-band, and its insertion loss level is about −4 dB, so it is not very useful. In [23], four isolation resistors and four sections of microstrip lines with various characteristic impedances and lengths make up the proposed PD. All PD variables are calculated using a genetic algorithm. In [24], to design a WPD, a new neuro-based approach based on a feed-forward neural network is proposed. In the typical configuration, quarter-wave transmission lines are replaced by symmetrical modified T-shaped resonators in the proposed PD.

Although these designs are suitable in isolation and matching, they often have limited bandwidth. They are large, and it is still a great challenge for many designers and engineers to design and fabricate a small dual-band PD with broad bandwidth.

The primary goal of this paper is to present a dual-band PD with small dimensions and suitable bandwidth, which uses a new low and high impedance stub to realize it. The design has a simplified and symmetrical architecture that can be easily implemented in microstrip technology. At working frequencies of 2.2 and 14.2 GHz, the proposed PD has more than 17 dB input reflection coefficients on all ports. It also has small dimensions and high fractional bandwidth (FBW). The simulated and measured results are compared and found to be highly correlated. To our knowledge, a dual-band PD in the S and Ku bands has never been designed before, and for the first time using the PSO algorithm, a new high and low impedance stub has been considered for use in a dual-band PD. Therefore, it can be used in radars, satellites, and many wireless applications.

Design procedure

The following is a breakdown of the steps involved in designing a dual-band WPD with a compact size and high bandwidth:

(1) Design a modified circuit for WPD: The first step is to consider the new arrangement of transmission lines to attain a new WPD.
(2) Calculation of line impedances and electrical lengths: The second step is performed using even and odd mode analysis and PSO algorithm to accurately calculate the values.

(3) WPD implementation: This is done using microstrip technology because it is less expensive and faster.
(4) Design of the WPD layout: In the structure of the modified WPD, low and high impedance stubs and symmetrical rectangular-shaped resonators are used instead of transmission lines.

Figure 1 depicts the conventional WPD, including 1/4 wavelength transmission lines and isolation resistance. Transmission lines 1/4 of the wavelength have an impedance of 70.7 Ω, an electrical length of 90°, and an isolation resistance of 100 Ω. Furthermore, all ports are matched with a 50 ohm resistance [3].

The conventional design has drawbacks, such as low S_{11} and small bandwidth. It is a single band that ignores any extra harmonics.

In this paper, instead of the transmission lines of each branch of the conventional design, a modified circuit, shown in Fig. 2, is used to create a dual-band structure and the appropriate bandwidth.

Nine transmission lines are used in the modified circuit, and its equivalent impedance is the same as the original structure's impedance.

One of the methods of analyzing telecommunication circuits, especially the PD, is the even and odd mode analysis method. The even mode will be modeled as an open circuit, while the odd mode will be modeled as a short circuit, and this method will be used to calculate line impedances and electrical lengths.

Odd mode analysis

The voltage in the middle of the circuit is zero in the excitation of the odd mode. As a result, the circuit can be divided into two halves by connecting the middle plate to the ground.

The equivalent circuit of the suggested PD in odd mode is shown in Fig. 3. The input and output ports' impedance are indicated by Z_0, and R is the isolation resistance between the output ports.

The following formulas for equivalent impedance under odd mode excitation can be derived using the high-frequency transmission line model:

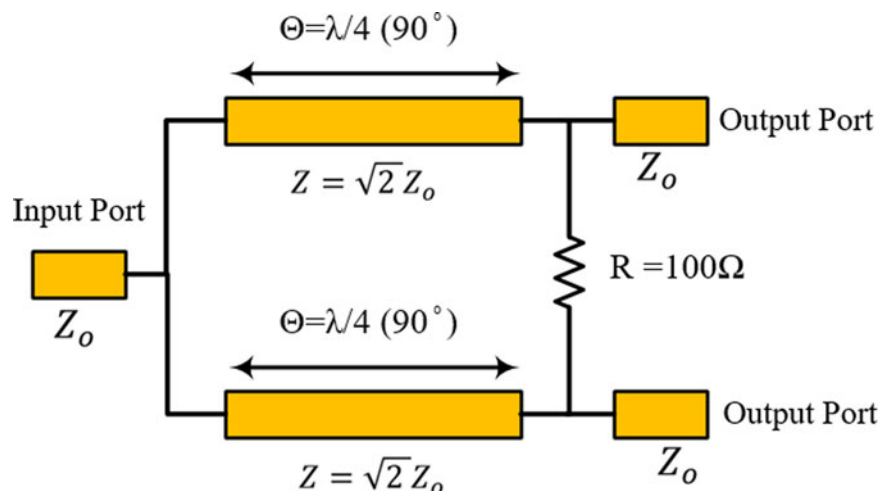$$z_{o7} = jz_7 \tan \theta_7 \tag{1}$$

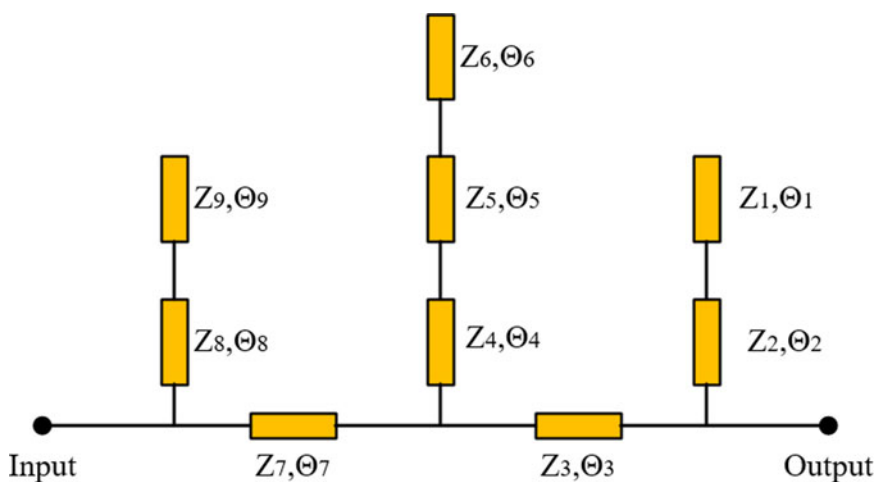**Fig. 1.** The conventional WPD [3].

Fig. 2. The proposed modified circuit.

$$z_{o6} = -jz_6 \cot \theta_6 \tag{2}$$

The characteristic impedance of the closed-end transmission line is calculated as equation (1), and to obtain the characteristic impedance of the open-end transmission line, its relation is as equation (2) [1].

$$z_{o5} = z_5 \frac{z_{o6} + jz_5 \tan \theta_5}{z_5 + jz_{o6} \tan \theta_5} \tag{3}$$

$$z_{o4} = z_4 \frac{z_{o5} + jz_4 \tan \theta_4}{z_4 + jz_{o5} \tan \theta_4} \tag{4}$$

Equation (5) shows the equivalent impedance of two parallel transmission lines.

$$z_{o3'} = \frac{z_{o4} \times z_{o7}}{z_{o4} + z_{o7}} \tag{5}$$

$$z_{o3} = z_3 \frac{z_{o3'} + jz_3 \tan \theta_3}{z_3 + jz_{o3'} \tan \theta_3} \tag{6}$$

Based on the equations of the high-frequency transmission line, the equivalent impedances of each section are calculated from left to right.

$$z_{o1} = -jz_1 \cot \theta_1 \tag{7}$$

$$z_{o2} = z_2 \frac{z_{o1} + jz_2 \tan \theta_2}{z_2 + jz_{o1} \tan \theta_2} \tag{8}$$

$$z_{o'} = \frac{Z_{o3} \times Z_{o2}}{Z_{o3} + Z_{o2}} \tag{9}$$

$$z_{eq-odd} = \frac{z_{o'} \times \dfrac{R}{2}}{z_{o'} + \dfrac{R}{2}} \tag{10}$$

In equation (10), z_{eq-odd} is the equivalent impedance of the odd mode on the right side of Fig. 3. Therefore, the derived
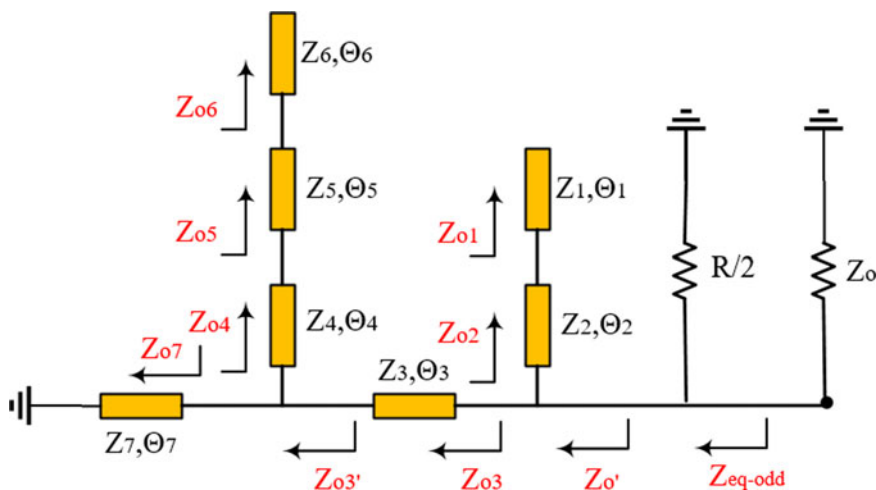

Fig. 3. The schematic of the equivalent odd-mode half circuit.

reflection coefficient Γ_{out}^{odd} at the output ports is expressed as follows:

$$\Gamma_{out}^{odd} = \frac{z_{eq-odd} - Z_0}{z_{eq-odd} + Z_0} \qquad (11)$$

The matching impedance is:

$$Z_0 = \frac{R}{2} \qquad (12)$$

Even mode analysis

In the excitation of the even mode, no current flows through the isolation resistor. As shown in Fig. 4, the whole structure can be bisected in half symmetrically in the horizontal direction. In this mode, the input port is 100 ohms, and the isolation resistor does not affect transmission performance. Figure 4 depicts the proposed PD's equivalent circuit in the even mode.

The method of calculating the equivalent impedance of the even mode is precisely the same as the odd mode and is based on the high-frequency transmission line equations. In the even mode analysis, the following equations represent the circuit equivalent impedance:

$$z_{e9} = -jz_9 \cot \theta_9 \qquad (13)$$

$$z_{e8} = z_8 \frac{z_{e9} + jz_8 \tan \theta_8}{z_8 + jz_{e9} \tan \theta_8} \qquad (14)$$

$$z_{e7'} = \frac{z_{e8} \times 2z_o}{z_{e8} + 2z_o} \qquad (15)$$

$$z_{e7} = z_7 \frac{z_{e7'} + jz_7 \tan \theta_7}{z_7 + jz_{e7'} \tan \theta_7} \qquad (16)$$

$$z_{e6} = -jz_6 \cot \theta_6 \qquad (17)$$

$$z_{e5} = z_5 \frac{z_{e6} + jz_5 \tan \theta_5}{z_5 + jz_{e6} \tan \theta_5} \qquad (18)$$

$$z_{e4} = z_4 \frac{z_{e5} + jz_4 \tan \theta_4}{z_4 + jz_{e5} \tan \theta_4} \qquad (19)$$

$$z_{e3'} = \frac{z_{e4} \times z_{e7}}{z_{e4} + z_{e7}} \qquad (20)$$

$$z_{e3} = z_3 \frac{z_{e3'} + jz_3 \tan \theta_3}{z_3 + jz_{e3'} \tan \theta_3} \qquad (21)$$

$$z_{e1} = -jz_1 \cot \theta_1 \qquad (22)$$

$$z_{e2} = z_2 \frac{z_{e1} + jz_2 \tan \theta_2}{z_2 + jz_{e1} \tan \theta_2} \qquad (23)$$

$$z_{eq-even} = \frac{z_{e2} \times z_{e3}}{z_{e2} + z_{e3}} \qquad (24)$$

Based on equation (24), $z_{eq-even}$ is the equivalent impedance of the even mode to the right side of Fig. 4. So, the derived reflection coefficient at the input port or the S_{11} parameter of the proposed PD can be calculated as follows:

$$S_{11} = \Gamma_{in}^{even} = \frac{z_{eq-even} - 2z_o}{z_{eq-even} + 2z_o} \qquad (25)$$

Next, to have a suitable WPD, the isolation between the output ports of the circuit must be zero ($S_{23} = 0$). Furthermore, for simplicity of design, the PD is assumed to be symmetric, so:

$$z_1 = z_9 \, . \, \theta_1 = \theta_9 \qquad (26)$$

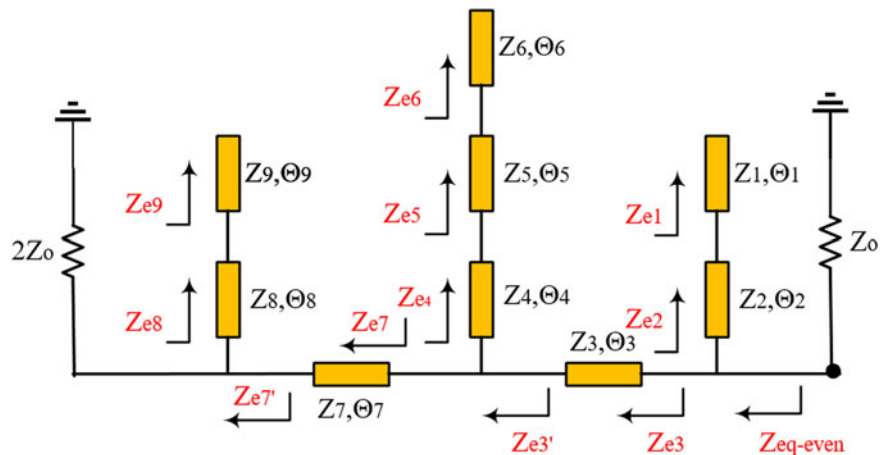$$z_2 = z_8 \, . \, \theta_2 = \theta_8 \qquad (27)$$

Fig. 4. The schematic of the equivalent even-mode half circuit.

$$z_3 = z_7 \,.\, \theta_3 = \theta_7 \tag{28}$$

The traditional PD structure has a characteristic impedance of $\sqrt{2}z_o$ and an electrical length of 90°. On the other hand, isolation I and the return loss of RL can be obtained as [25]:

$$I \text{ (dB)} = -20.\log|S_{23}| \tag{29}$$

$$RL(\text{dB}) = -20.\log\left|\frac{P_{in}}{p_{ref}}\right| \tag{30}$$

Return loss measures the efficiency with which power is delivered from a transmission line to a load. In equation (30), the power in the PD under test is P_{in}, and the reflected power to the source is p_{ref}.

For the real and imaginary parts of the S_{11}, a value close to zero (-0.17) is chosen to give a wide bandwidth. As a result, RL is greater than 17 dB, as expected.

Now, to have suitable matching and insertion losses at working frequencies (f_1, f_2), we must calculate the optimal values for the parameters z_{1-9} and θ_{1-9}. But equations (11) and (25) are very complicated and the number of problem variables is large, so it is impossible to solve them manually.

Optimization and calculation of design parameters

Due to its effectiveness in designing microwave circuits, the PSO method was utilized to find the best design parameters [26–28]. The objective function for optimal design is obtained as equation (31).

$$
\begin{aligned}
F = \min &\left[\sum_{i=1}^{2} \frac{\Gamma_{in(11)}.f(i)}{n} + \sum_{i=1}^{2} \frac{\Gamma_{in(23)}.f(i)}{n} + \sum_{i=1}^{2} \frac{\Gamma_{in(22)}.f(i)}{n} \right.\\
&\left. + \sum_{i=1}^{2} \frac{\Gamma_{in(33)}.f(i)}{n} \right] + \max\left[\sum_{i=1}^{2} \frac{\Gamma_{in(12)}.f(i)}{n} + \sum_{i=1}^{2} \frac{\Gamma_{in(13)}.f(i)}{n} \right]
\end{aligned}
\tag{31}
$$

Since our goal is to design a dual-band WPD, equation (31) is written in a two-part form. The input/output return coefficient and isolation parameters should be minimized in this objective function at the operating frequencies of the WPD, and insertion losses should be at maximum values. Therefore, the results obtained by applying these conditions are the optimal parameters of the WPD.

Also, the presented objective function contains six goals for two frequencies simultaneously. The search space of this optimization is large, the range of variables is extensive, and it will be complicated to find the most optimal values; thus, calculating them individually is impossible.

PSO algorithm

The PSO optimization algorithm is one of the most significant algorithms in the swarm intelligence field [29]. Due to its simplicity and effectiveness, the PSO algorithm has recently become very popular in designing high-frequency circuits and electromagnetic systems [30, 31]. The technique is inspired by the social behaviors of living animals, such as fish and birds, which dwell in small and large groups. In this algorithm, all population members connect with each other and solve the problem by exchanging information. Each member of the population is called a particle, and these particles are spread throughout the search space of the function that is being optimized. The position of each particle is checked by calculating the objective function. Then, a direction to move is chosen by utilizing the information from its present location and the best position it has ever been in, as well as the information from one or more of the best particles in the collection. After all the particles have updated their position, one step of the algorithm ends. These steps are repeated several times until the desired answer is obtained. A collection of particles seeking the most optimal value of a function is like a group of birds looking for food.

This algorithm's foundation may be summed up as follows: each particle modifies its position in the search space at each instant by the best place it has experienced thus far and the best place among its neighbors. Like other evolutionary computations, the PSO method begins with generating a random initial population. The initial population consists of N particles that are randomly initialized. Each particle has two position and velocity values, represented by position and velocity vectors. By determining the value of the objective function, these particles begin to move in the problem space and look for better positions. To search, each particle requires two memories. The best location of each particle in the past is stored in one memory, and the best place of all particles is stored in one memory. The particles decide how to move in the following step using information from these memories. All particles adjust their velocity and location in each iteration based on the best absolute and local solutions [32]. According to equation (32), the location of each particle in the population is computed by adding the velocity of the same particle to its present position.

$$X_k(i) = X_k(i-1) + V_k(i) \tag{32}$$

In equation (32), X is the position of particle number k, and V represents its speed. The number of repetitions is also indicated by i. The speed parameter advanced the optimization process, representing the particle's experimental knowledge and social information exchange with its neighbors. Equation (33) is used to compute speed.

$$
\begin{aligned}
V_k(i) = \theta(i).V_k(i-1) &+ c_1 r_1 [P_{best,k} - X_k(i-1)] \\
&+ c_2 r_2 [G_{best} - X_k(i-1)]
\end{aligned}
\tag{33}
$$

$V_k(i)$ is the ith component of the k-th particle velocity in equation (33). r_1 and r_2 are two random numbers with uniform distribution in the interval (0, 1).

The parameters c_1 and c_2 are individual and group learning factors, which usually choose $c_1 = c_2 = 2$ based on experimental results [32]. The best local place that the particle has attained so far is represented by $P_{best,k}$, and the best global place that all particles have achieved thus far is indicated by G_{best}.

According to equation (34), $\theta(i)$ or inertia weight is employed to control the speed of particles during test repetitions [33].

$$\theta(i) = \theta_{\max} - \left(\frac{\theta_{\max} - \theta_{\min}}{i_{\max}}\right)i \tag{34}$$

$\theta_{\min}$ or $\theta_{\max}$ are the initial and final values of the inertia weight, respectively. The algorithm's maximum iteration number is indicated by $i_{\max}$. It has been demonstrated via experimentation

Table 1. Elective parameters of PSO for optimizing this article

PSO parameters	the PSO algorithm's selected values
N	40
θ_{max}	0.7
θ_{min}	0.4
i_{max}	300
c_1	2
c_2	2

Table 2. Calculated values for z and θ of the proposed WPD based on the PSO algorithm (units: z: Ω; θ: °)

z_1	θ_1	z_2	θ_2
32.89	7.04	164.3	12.1
z_3	θ_3	z_4	θ_4
105	0.33	18.26	2.5
z_5	θ_5	z_6	θ_6
19.7	2.15	167.57	4.25
R			
100 Ω			

that for θ_{min} and θ_{max}, the optimal solution to the optimization issue will often be found if the values are $\theta_{min} = 0.4$ and $\theta_{max} = 0.7$ [34].

Optimization of design parameters

The PSO algorithm's specified parameters, which are listed in Table 1, have been used to optimize the design parameters for this article.

Based on the relations and the objective function introduced in equation (31), the results of the PSO algorithm for electrical impedances and lengths are presented in Table 2.

Implementation

One of the methods of implementing the proposed circuit is using microstrip lines in which the conductor is separated from the ground by a dielectric layer called the substrate. This technology is used to transmit RF frequency signals. So, in this article, instead of transmission lines, two high and low impedance stubs and symmetrical resonators have been used to improve and upgrade the PD compared to the conventional type.

Design of high and low impedance stub

Instead of wavelength 1/4 transmission lines in the conventional WPD, the proposed structure uses a combination of two
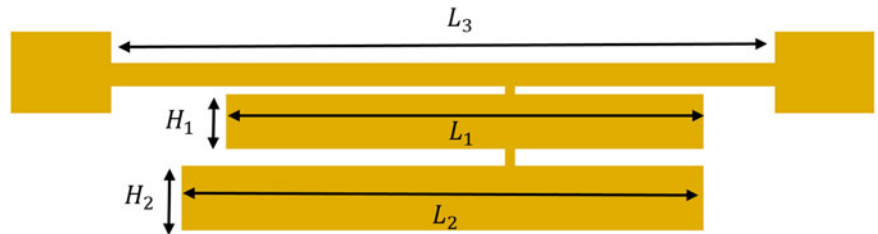

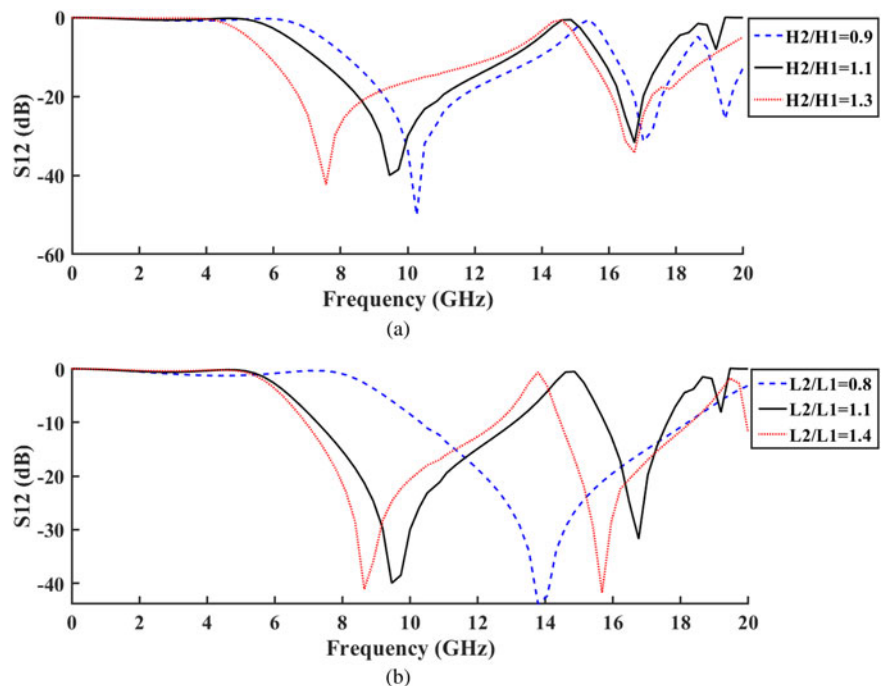**Fig. 5.** The proposed high and low impedance stub.

Fig. 6. The simulated S_{12} of the presented stub as a function of (a) H2/H1, (b) L2/L1.
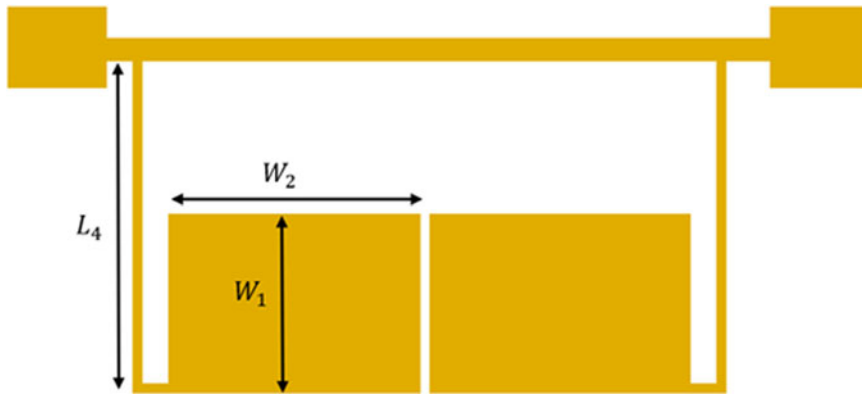
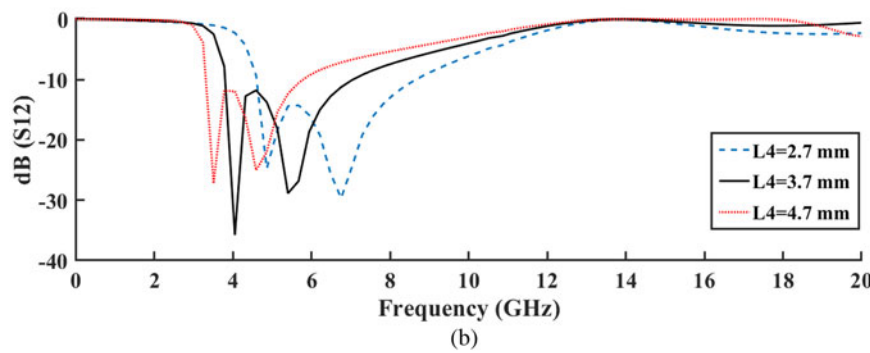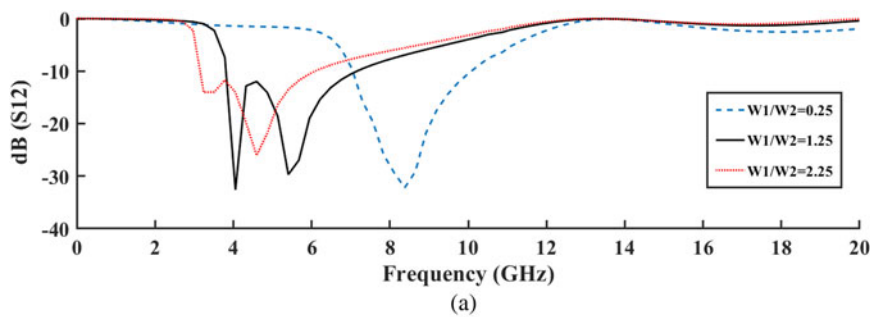**Fig. 7.** The layout of rectangular-shaped resonators.

Fig. 8. The simulated S_{12} of the presented rectangular-shaped resonator as a function of (a) W1/W2, (b) L4.

Fig. 9. The proposed power divider's layout.

symmetrically compressed microstrip resonators and a novel high and low impedance stub. Figure 5 shows the high and low impedance stubs that have replaced the impedances z_4, z_5, and z_6. A high and low impedance stub is employed to produce frequency responses with a broad stop-band bandwidth.

In the following, the dimensions of the presented stub are changed, and their effect on the simulation results is investigated.

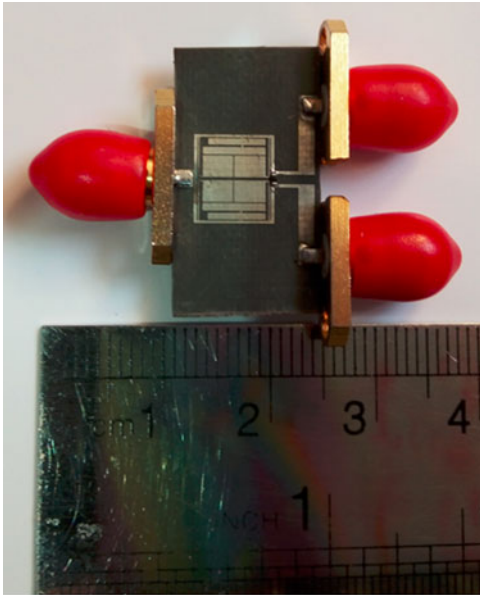Figures 6(a) and 6(b) depict insertion loss (S_{12}) for various H2/H1 and L2/L1 values, respectively.

Fig. 10. Photograph of the fabricated dual-band WPD.

The proposed stub produces two transmission zeros in the S_{12} result, as shown in Figs 6(a) and 6(b), and changing the stub dimensions shifts the location of the transmission zeros. Because of this change, the bigger the high impedance stub, the smaller the resonant frequency, and vice versa. Therefore, the designed structure has high flexibility, and it is easy to control the transmission zeros created by it.

Since this stub alone cannot create broad or multiple rejection bands, as shown in Fig. 2, other transmission lines must be added next to it.

Design of symmetrical resonators

Figure 7 shows results that illustrate how symmetrical resonators can produce a dual-band circuit by filtering out undesired signals. Compact microstrip cells are employed as the resonators, and in place of impedances, z_{1-2} and z_{8-9} are located. These resonators are rectangular-shaped and have inductive properties, resulting in transmission zeros in the frequency response and improved circuit performance.

The transmission zero created by the resonators is shifted by changing the length and width of the resonator bases, and the transmission zero reduces as the length of the resonator bases increases. Figures 8(a) and 8(b) show the resonator simulation results. As can be seen, when $W1/W2 = 1.25$ and $L4 = 3.7$ mm, the optimal conditions for these resonators are obtained, and a wide stop-band bandwidth is created in the S_{12} result.

Based on the simulation results, a dual-band circuit can be created by combining the symmetrical resonators with the high and low impedance stub. The resonators produce the first pass band, and the stub produces the second pass band. A broader stop-band is also produced by transmission zeros

Final structure

The final PD layout is depicted in Fig. 9. This structure combines high and low impedance stubs and rectangular-shaped resonators compactly positioned to prevent dimension increase. It will replace transmission lines in the modified WPD structure. The optimal dimensions for the high and low impedance stub to create a dual-band WPD with central frequencies of 2.2 and 14.2 GHz are as follows (all in mm):

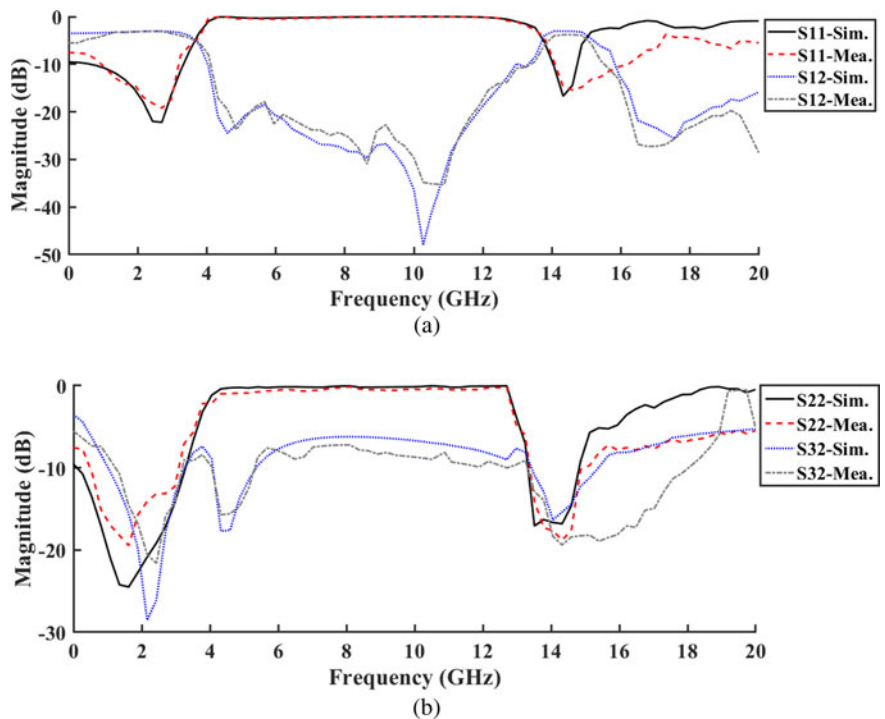$$L_1 = 5.3, \ L_2 = 5.8, \ L_3 = 6.8, \ H_1 = 0.6, \ \text{and} \ H_2 = 0.7$$

Fig. 11. Simulated and measurement results of designed WPD (a) S_{11} and S_{12}, (b) S_{22} and S_{32}.
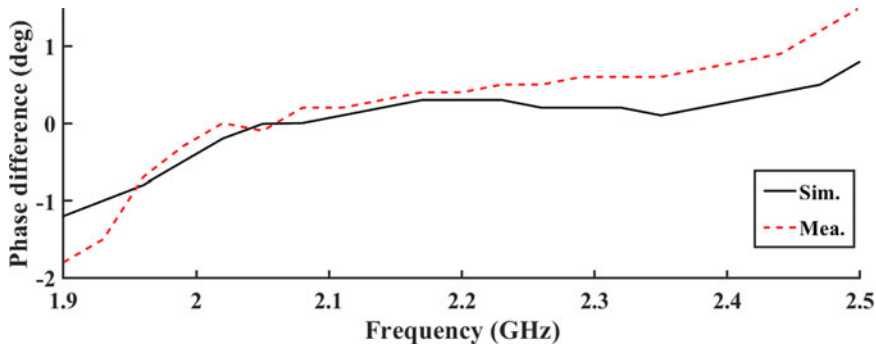
Fig. 12. Simulated and measured (a) phase difference and (b) amplitude difference between output ports.
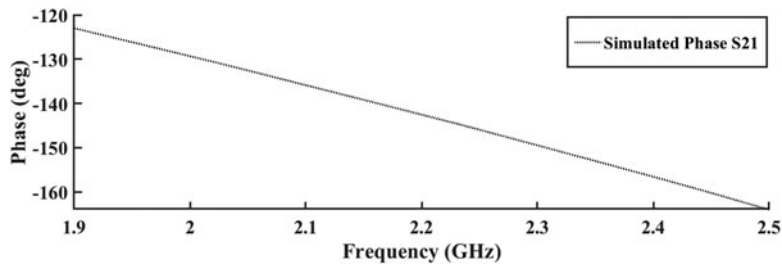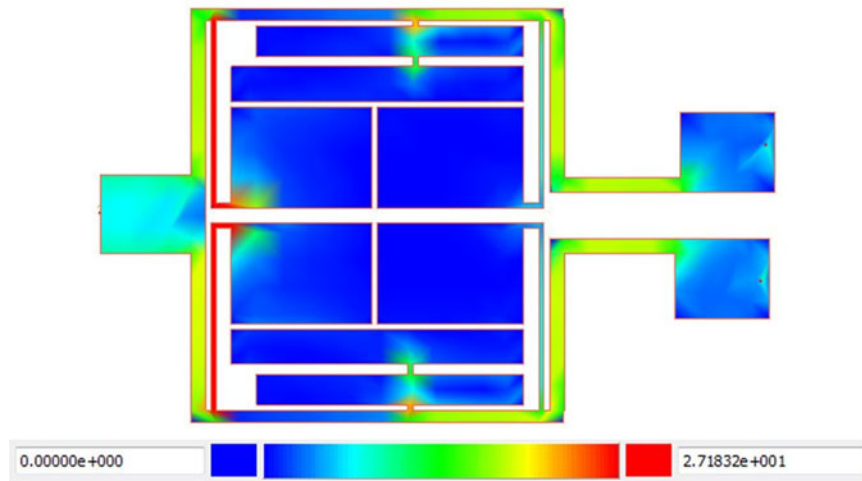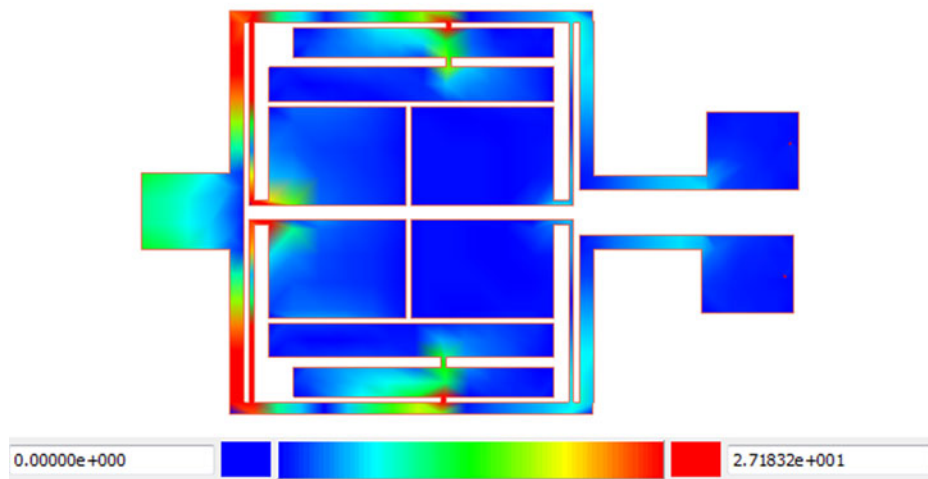

Fig. 13. Simulation results of phase difference between input and output ports.

(a)

(b)

Fig. 14. The current distribution profile of the proposed WPD at (a) 2.2 GHz and (b) 10 GHz.

The substrate intended for the layout design is RT Duroid 5880 with a thickness of 20 mil, $\epsilon_r = 2.2$, and the dielectric loss tangent is 0.0009. The fabricated circuit is shown in Fig. 10, and its total size is 7.4 mm × 8.1 mm ($0.072 \lambda_g \times 0.079 \lambda_g$).

Figures 11(a) and 11(b) show a comparison of circuit measurement and electromagnetic (EM) simulation. The simulation results were obtained using ADS software, and the measurement was performed with Agilent network analyzer N5230A.

The central frequencies of the two wide passbands in the proposed circuit are 2.2 and 14.2 GHz. The S_{11} is −22.1 and −17 dB in these operating frequencies, respectively. As is observed, for the proposed WPD, an appropriate reject band is obtained, 4.4–11.5 GHz, which can suppress 2nd up to 5th unwanted harmonics (−25, −28, −27, −33, and −18 dB). In addition, insertion losses (S_{21}) are −3.07 and −3.1 dB in the operating frequencies. Isolation (S_{23}) and reflection coefficient in output ports (S_{22} or S_{33}) simulation results are shown in Fig. 11(b). In the operating frequencies, isolation between output ports is better than 20 dB, and the reflection coefficient of the output port is more than 17 dB. The FBW obtained by considering −15 dB as the attenuation level is 54.5% for the first

band and 20.1% for the second band. So, there is a wide stop-band and good sharpness in the proposed WPD output results.

In the second working frequency, there are more losses due to the change in the loss tangent of the substrate. Moreover, the simulated and measured results are highly consistent, and their minor differences are due to measurement errors.

One of the significant advantages of the designed WPD is the high distance between the operating frequency bands, which makes it possible to use this circuit in various applications.

The phase and amplitude differences of the two isolated ports are shown in Figs 12(a) and 12(b), respectively. The phase difference around the operating frequency is less than 2 degrees, and the amplitude difference between output ports is less than 0.1 dB, indicating that the proposed circuit splits power evenly between the output ports and is entirely symmetrical.

In the final fabricated circuit, the two output 50 ohm transmission lines have different lengths from the input 50 ohm transmission line. So, to check the performance of the microstrip lines and their effects, the phase difference between the input and output ports around the central frequency is shown in Fig. 13.

Table 3. Comparison with previous studies

Ref.	Working frequency (GHz)	Design	Optimization algorithm	FBW/RL (%)	IL (dB)	Size ($\lambda g \times \lambda g$)	Nth harmonics suppression
[5]	3.5/5	Stub-loaded resonators	No	7.4/4.2	3.9/4.9	0.27 × 0.35	–
[9]	2.6/5.7	Circular patch resonator	No	25/10	3.6/4.2	0.72 × 0.72	2nd
[17]	0.9/2.45	Short-circuited composite right-/left-handed stub	No	33/8	3.19/3.18	0.11 × 0.16	–
[19]	0.50/2.50	Series stub	No	20/12	3.25/4.49	0.23 × 0.07	–
[22]	4.2[a]	Open-circuit T-shaped resonators	Yes	1.15	4.1	0.35 × 0.73	–
[23]	6.9[a]	Four sections of microstrip lines and four isolation resistors	Yes	38	3.2	NA	2nd
[24]	1.74[a]	T-shaped resonators	Yes	40	3.3	0.11 × 0.13	5th
[35]	2.45[a]	Microstrip gap-coupled resonators	Yes	28	3.3	0.7 × 0.62	–
[36]	0.5[a]	Non-uniform transmission lines	Yes	25	3.36	NA	–
[37]	1.3/2.08	Varactor-based	No	4.8/7.7	5.4/4.8	0.14 × 0.23	–
[38]	0.9/2.1	Stepped-impedance resonators	No	22/9.5	3.2/3.4	0.26 × 0.20	2nd
[39]	2.45/5.13	Coupled lines	No	58.3/17.8	3.89/4.39	0.3 × 0.29	–
[40]	1/2	Coupled lines	No	31.6/18.2	3.1/3.2	0.47 × 0.38	–
[41]	1.8/2.96	Band-pass filter	No	8/7.4	3.8/3.9	NA	3rd
[42]	1/2.6	Frequency-dependent complex load	No	16/13.1	3.2/3.6	0.106 × 0.11	–
[43]	1.61/2.49	Dual-composite right/left-handed resonators	No	NA	3.55/3.9	0.33 × 0.35	–
This work	2.2/14.2	Low and high impedance stub and rectangular-shaped resonators	Yes	54.5/20.1	3.07/3.1	0.072 × 0.079	5th

[a]Single-band.

The current distribution profile of the proposed WPD at 2.2 and 10 GHz is shown in Figs 14(a) and 14(b), respectively, which depict how resonators cause resonance at desired frequencies. According to Fig. 14(a), there is a high electrical current distribution at the output ports that is evenly led between them. But at 10 GHz, electromagnetic waves enter the PD from port 1 and are blocked by resonators when passing through transmission lines. These simulations also demonstrate that the designed PD is symmetric and can be well used at operating frequencies.

Table 3 represents a comparison between the proposed WPD with the previous works. It confirms that the proposed WPD is one of the best structures presented to date because it has the smallest dimensions, suppresses five undesired harmonics, and has a high FBW. It is pertinent to note that our design has the best insertion loss among other recent state-of-the-art works.

The proposed WPD operates at 2.2 and 14.2 GHz frequencies and covers two frequency bands. As a result, it applies to all *S*-band and Ku-band devices; for example, medical sensors, smartphone processors, radars for airport security, weather radars, surface ship radars, communications satellites, etc.

Conclusion

This paper proposed a dual-band WPD with 2.2 and 14.2 GHz central frequencies. This PD comprises two similarly rectangular-shaped resonators and new high and low impedance stubs, which minimizes the size while simultaneously creating a wide cut-off bandwidth. In addition, the proposed circuit's characteristic impedances and electrical lengths were analyzed using odd and even mode analysis, and the optimal values were obtained using the PSO algorithm. This proposed PD can divide signals into various microwave amplifiers, antenna arrays, and mixers.

References

1. **Pozar DM** (2011) *Microwave Engineering*, 4th Ed. New York: Wiley.
2. **Abu-Alnadi O, Dib N, Al-Shamaileh K and Sheta A** (2015) Design and analysis of unequal split Bagley power dividers. *International Journal of Electronics* **102**, 500–513.
3. **Wilkinson EJ** (1960) An N-way hybrid power divider. *IRE Transactions on Microwave Theory and Techniques* **8**, 116–118.
4. **Wang X, Ma Z, Sakagami I, Yoshikawa M and Mase A** (2015) Wilkinson power divider with band-pass filter response and easy structure. *Asia-Pacific Microwave Conference (APMC)* **3**, 1–3. https://doi.org/10.1109/APMC.2015.7411797.
5. **Li Q, Zhang Y and Fan Y** (2015) Dual-band in-phase filtering power dividers integrated with stub-loaded resonators. *Microwave Antennas Program* **9**, 695–699.
6. **Zonouri SA and Hayati M** (2019) A compact ultra-wideband Wilkinson power divider based on trapezoidal and triangular-shaped resonators with harmonics suppression. *Microelectronics Journal* **89**, 23–29.
7. **Imani MS and Hayati M** (2021) Compact Wilkinson power divider with extensive suppression of harmonics, using a combination of trapezoidal, circular and rectangular resonators. *AEU-International Journal of Electronics and Communications* **139**, 153935.
8. **Zhang Q, Zhang G, Liu Z, Tan X, Tang W and Yang H** (2021) A new balanced-to-single-ended in-phase filtering power divider based on circular patch resonator with good isolation and wide stopband. *International Journal of RF and Microwave Computer-Aided Engineering* **31**, e22839.
9. **Zhang Q, Zhang G, Liu Z, Chen W and Tang W** (2021) Dual-band filtering power divider based on a single circular patch resonator with improved bandwidths and good isolation. *IEEE Transactions on Circuits and Systems II: Express Briefs* **68**, 3411–3415. https://doi.org/10.1109/TCSII.2021.3081266.
10. **Xu K, Xu J and Li D** (2019) Wilkinson filtering power divider using coupled lines and T-shaped stub. *Microwave and Optical Technology Letters* **61**, 2540–2544.
11. **Bei L, Zhang L and Huang K** (june 2021) A novel microstrip array circular polarized antenna based on t-type power divider. *Wireless Networks*, 1–7. https://doi.org/10.1007/s11276-021-02658-3.
12. **Habibi H and Miar Naimi H** (2019) Taper transmission line UWB Wilkinson power divider analysis and design. *International Journal of Electronics* **106**, 1332–1343.
13. **Xia B, Cheng J-D, Wu L-S, Xiong C and Mao J-F** (2020) A new compact power divider based on capacitor central loaded coupled microstrip line. *IEEE Transactions on Microwave Theory and Techniques* **68**, 4249–4256.
14. **Chen S, Yu Y and Tang M** (2019) Dual-band Gysel power divider with different power dividing ratios. *IEEE Microwave and Wireless Components Letters* **29**, 462–464.
15. **Wu H, Sun S, Wu Y and Liu Y** (2020) Dual-band Gysel power dividers with large frequency ratio and unequal power division. *International Journal of RF and Microwave Computer-Aided Engineering* **30**, e22203.
16. **Zonouri SA and Hayati M** (2021) A compact Gysel power divider with ultra-wide rejection band and high fractional bandwidth. *International Journal of RF and Microwave Computer-Aided Engineering* **31**, e22643.
17. **Zhao M, Kumar A, Wang C, Xie B, Qiang T and Adhikari KK** (2019) Design method of dual-band Wilkinson power divider with improved out-of-band rejection performance and high design flexibility. *AEU-International Journal of Electronics and Communications* **110**, 152844.
18. **Zhang G, Wang J, Zhu L and Wu W** (2016) Dual-band filtering power divider with high selectivity and good isolation. *IEEE Microwave and Wireless Components Letters* **26**, 774–776.
19. **Jaradat H, Dib N and Al Shamaileh K** (2019) Miniaturized dual-band CPW Wilkinson power divider using T-network adopting series stubs with a high frequency ratio. *AEU-International Journal of Electronics and Communications* **107**, 32–38.
20. **Zhang H, Kang W and Wu W** (2016) Design of a novel compact dual-band Wilkinson power divider with improved isolation. *2016 IEEE International Conference on Microwave and Millimeter Wave Technology (ICMMT)*, IEEE, vol. 2, pp. 976–978. https://doi.org/10.1109/ICMMT.2016.7762505.
21. **Bemani M and Nikmehr S** (2016) Dual-band 3-way power divider and combiner based on CRLH-TLs. *International Journal of Microwave and Wireless Technologies* **8**, 1037–1043.
22. **Dadgarpour A, Dadashzadeh G, Naser-Moghadasi M, Jolani F and Virdee BS** (2010) PSO/FDTD optimization technique for designing UWB in-phase power divider for linear array antenna application. *IEEE Antennas and Wireless Propagation Letters* **9**, 424–427.
23. **Wang H, Tang X, Liu Y and Cao Y** (2012) Analysis and design of ultra-wideband power divider by micro-genetic algorithm. *Journal of Electromagnetic Waves and Applications* **26**, 1341–1349.
24. **Jamshidi M, Lalbakhsh A, Lotfi S, Siahkamari H, Mohamadzade B and Jalilian J** (2020) A neuro-based approach to designing a Wilkinson power divider. *International Journal of RF and Microwave Computer-Aided Engineering* **30**, e22091.
25. **Bird TS** (2009) Definition and misuse of return loss [report of the transactions editor-in-chief]. *IEEE Antennas and Propagation Magazine* **51**, 166–167.

26. **Wang WB, Feng Q and Liu D** (2012) Synthesis of thinned linear and planar antenna arrays using binary PSO algorithm. *Progress in Electromagnetics Research* **127**, 371–387.

27. **Chatterjee A, Mahanti GK and Mahanti A** (2015) Synthesis of thinned concentric ring array antenna in predefined phi-planes using binary firefly and binary particle swarm optimization algorithm. *International Journal of Numerical Modelling: Electronic Networks, Devices and Fields* **28**, 164–174.

28. **Liu G, Zhang H and Li Z** (2021) Pixelated microwave sensor for angular displacement detection. *2021 13th International Symposium on Antennas, Propagation and EM Theory (ISAPE)*, IEEE, pp. 1–3. https://doi.org/10.1109/ISAPE54070.2021.9753437.

29. **Kennedy J and Eberhart R** (1995) Particle swarm optimization. *Proceedings of ICNN'95–International Conference on Neural Networks*, IEEE, Vol. 4, pp. 1942–1948. https://doi.org/10.1109/ICNN.1995.488968.

30. **Luo X, Yang B and Qian HJ** (2018) Adaptive synthesis for resonator-coupled filters based on particle swarm optimization. *IEEE Transactions on Microwave Theory and Techniques* **67**, 712–725.

31. **Verma RK and Srivastava DK** (2019) Design, optimization and comparative analysis of T-shape slot loaded microstrip patch antenna using PSO. *Photonic Network Communications* **38**, 343–355.

32. **Shi Y and Eberhart R** (1998) A modified particle swarm optimizer. *1998 IEEE International Conference on Evolutionary Computation Proceedings. IEEE World Congress on Computational Intelligence (Cat. No. 98TH8360)*, IEEE, pp. 69–73. https://doi.org/10.1109/ICEC.1998.699146.

33. **Shi Y** (2001) Particle swarm optimization: developments, applications and resources. *Proceedings of the 2001 Congress on Evolutionary Computation (IEEE Cat. No. 01TH8546)*, IEEE, Vol. 1, pp. 81–86. https://doi.org/10.1109/CEC.2001.934374.

34. **Eberhart RC and Shi Y** (2000) Comparing inertia weights and constriction factors in particle swarm optimization. *Proceedings of the 2000 Congress on Evolutionary Computation. CEC00 (Cat. No. 00TH8512)*, IEEE, Vol. 1, pp. 84–88. https://doi.org/10.1109/CEC.2000.870279.

35. **Chen S and Wu TL** (2020) A fully integrated arbitrary power divider on printed circuit board by a novel SMD-resistor-free isolation network. *IEEE Transactions on Components, Packaging and Manufacturing Technology* **10**, 1889–1901.

36. **Hosseini F, Khalaj-Amir Hosseini M and Yazdani M** (2009) A miniaturized Wilkinson power divider using nonuniform transmission line. *Journal of Electromagnetic Waves and Applications* **23**, 917–924.

37. **Chi P-L and Yang T** (2016) A 1.3–2.08 GHz filtering power divider with bandwidth control and high in-band isolation. *IEEE Microwave and Wireless Components Letters* **26**, 407–409.

38. **Shao C, Li Y and Chen J** (2017) Compact dual-band microstrip filtering power divider using T-junction structure and quarter-wavelength SIR. *Electronics Letters* **53**, 434–436.

39. **Feng T, Ma K and Wang Y** (2020) A dual-band coupled line power divider using SISL technology. *IEEE Transactions on Circuits and Systems II: Express Briefs* **68**, 657–661.

40. **Maktoomi MH, Banerjee D and Hashmi MS** (2017) An enhanced frequency-ratio coupled-line dual-frequency Wilkinson power divider. *IEEE Transactions on Circuits and Systems II: Express Briefs* **65**, 888–892.

41. **Li YC, Xue Q and Zhang XY** (2012) Single-and dual-band power dividers integrated with bandpass filters. *IEEE Transactions on Microwave theory and Techniques* **61**, 69–76.

42. **Gupta R, Gabdrakhimov B, Dabarov A, Nauryzbayev G and Hashmi MS** (2021) Development and thorough investigation of dual-band Wilkinson power divider for arbitrary impedance environment. *IEEE Open Journal of the Industrial Electronics Society* **2**, 401–409.

43. **Huang T, Feng L, Geng L, Liu H, Zheng SY, Ye S, Zhang L, and Xu H** (2021) Compact dual-band Wilkinson power divider design using via-free D-CRLH resonators for Beidou navigation satellite system. *IEEE Transactions on Circuits and Systems II: Express Briefs* **69**, 65–69.

Seyed Abed Zonouri received the B.Sc. degree in control engineering from the Shahid Beheshti University, Tehran, Iran, in 2016 and M.Sc. degree in electronic engineering in 2019 from Razi University of Kermanshah. He is currently a Ph.D. candidate in Electrical Department at Razi University, Kermanshah, since 2020. His research interests include high-frequency circuit design, microwave components, and nano structures.

Mohsen Hayati received the B.E. degree in electronics and communication engineering from Nagarjuna University, Andhra Pradesh, India, in 1985, and the M.E. and Ph.D. degrees in electronics engineering from Delhi University, Delhi, India, in 1987 and 1992, respectively. He joined the Electrical Engineering Department, Razi University, Kermanshah, Iran, as an assistant professor in 1993. Currently, he is a professor with the Electrical Engineering Department, Faculty of Engineering, Razi University. He has published more than 300 papers in international, domestic journals, and conferences. His current research interests include microwave and millimeter wave devices and circuits, power amplifiers, low noise amplifier design, analog cmos circuit, application of computational intelligence, artificial neural networks, fuzzy systems, neuro-fuzzy systems, electronic circuit synthesis, modeling, and simulations.

Mehran Bahrambeigi obtained B.Sc. and M.Sc. in electronic engineering from Razi University, Kermanshah, Iran in 2008 and 2022, respectively. His research interests focus on microstrip coupler and filter, microwave power dividers filter, and neural networks.